RSC Advances

PAPER

View Article Online
View Journal | View Issue

Cite this: *RSC Adv.*, 2017, **7**, 22627

Ethanol sensor development based on ternary-doped metal oxides (CdO/ZnO/Yb_2O_3) nanosheets for environmental safety†

Mohammed M. Rahman,[ab] M. M. Alam,*[c] Abdullah M. Asiri[ab] and M. A. Islam[c]

Received 14th February 2017
Accepted 10th April 2017

DOI: 10.1039/c7ra01852e

rsc.li/rsc-advances

Herein, we report the construction of a dynamic, highly sensitive, stable, reliable, and reproducible selective ethanol sensor based on a ternary metal oxide system of CdO/ZnO/Yb_2O_3 nanosheets (NSs). The NSs were synthesized by a hydrothermal process in alkaline phases. The morphological and structural characterization of the synthesized NSs were approved using various advantageous and well-established conventional methods such as Fourier-transform infrared spectroscopy (FTIR), ultraviolet visible spectroscopy (UV/vis), field emission scanning electron microscopy (FESEM), X-ray photoelectron spectroscopy (XPS), energy-dispersive X-ray spectroscopy (EDS), and powder X-ray diffraction (XRD). A thin layer of CdO/ZnO/Yb_2O_3 NSs was deposited onto a glassy carbon electrode (GCE) with conducting binder to produce a working electrode. A calibration plot was obtained and was found to be linear over the ethanol concentration range (linear dynamic range, LDR) from 0.35 nM to 3.5 mM with the detection limit (LoD) of 0.127 ± 0.006 nM and the quantification limit (LoQ) of 0.423 ± 0.02 (signal-to-noise ratio, at the S/N of 3), and the system exhibited a sensitivity of 7.4367 μA mM^{-1} cm^{-2}. Furthermore, the proposed chemical sensor was successively applied for the detection of ethanol in various environmental samples. This approach was introduced as a well-organized route for efficient ethanol sensor development in environmental and health-care fields in a broad scale.

Introduction

Recent developments in advanced nanotechnology and in innovative chemi-sensors, nanomaterials, and nanodevices have been regulating a key task in the fabrication and improvement of very precise, perceptive, accurate, sensitive, and consistently efficient chemical sensors. The exploration for even small electrodes accomplished in nano-level imaging and in controlling doped nanomaterials, doping agents (host–guest), biological, chemical, pathological samples, and chemical sensors has extended scientists awareness for control monitoring, especially in the fields of environmental safety and health monitoring. Recently, significant attention has been focused on the detection of toxic chemicals in regard to human health and to the ecological system to prevent and reduce the harmful effects of toxic chemicals.[1] Ethanol is extensively used as a solvent in the biomedical, chemical, food, and alcoholic beverages industries,[2] but it is also a hypnotic (sleep producer) chemical, slightly toxic in nature, inflammable, and colorless. The exposure of ethanol may cause some health problems such as headache, drowsiness, irritation of eyes, and difficulty in breathing.[3] Heavy exposure or consumption of ethanol, particularly by smokers, increases the risk of cancer in the upper respiratory and digestive paths, as well as causing liver damage, and among women, there is a possibility of breast cancer. Workers in the ethanol industry have an increased risk of suffering from respiratory and digestive track cancer. Consumption of ethanol in the form of alcohol has many issues such as drunk driving that can cause traffic accidents and is a serious problem in society. Therefore, an ethanol sensor would also be very important for public transportation systems.[4] Consequently, it is a great ultimatum and emergent challenge for detecting ethanol even at the very trace level.[5] A variety of analytical techniques, such as hydrometric, gas/liquid chromatography, refractometry, and infrared spectroscopy, have been utilized for ethanol detection.[6] Nowadays, the electrochemical technique is considered the major detection method for hazardous toxics as it has many great advantages, such as high selectivity, a wide linear range, economical sustainability, rapid responses, portability, and a simple operating procedure.[7] However, this technique has a number of difficulties and issues, such as a need to improve the electron transfer rate between the surface of the working electrode of the sensors and the analytes. Therefore, depending on the electrochemical and current–voltage

[a]*Chemistry Department, King Abdulaziz University, Faculty of Science, P.O. Box 80203, Jeddah 21589, Saudi Arabia*

[b]*Center of Excellence for Advanced Material Research (CEAMR), King Abdulaziz University, P.O. Box 80203, Jeddah 21589, Saudi Arabia*

[c]*Department of Chemical Engineering and Polymer Science, Shahjalal University of Science and Technology, Sylhet 3100, Bangladesh. E-mail: mmalamsust@gmail.com; Tel: +880-01711587246*

† Electronic supplementary information (ESI) available. See DOI: 10.1039/c7ra01852e

(*I–V*) characteristics, directly grown nanostructures comprising transition metal oxides on the expected electrode should be favorable for the reliable and effective identification of toxic chemicals and biochemical species.[8] To progress the functionalities and sensitivities of the sensors, presently electron mediators are utilized that help fast electron transfer between the surface of the anticipating electrode and the analytes.[9]

Doped nanostructure materials of transition metal oxides and semiconductors have attracted much interest owing to their technological applications and exciting optical and structural properties. The distinctive physical and chemical properties of nanomaterials due to their surface as well as size/shape effects means that doped materials have been explored in much research, in terms of both scientific importance and industrial applications. Therefore, semiconductor metal oxides-based sensors have attracted distinctive attention due to their diversified applications in environmental monitoring, chemical process control, personal safety, health care, defense, security, and so on.[10,11] Sensors based on semiconductor nanostructured metal oxides have great benefits because of their small dimensions, low cost, low power consumption, simple processing, and good stability.[12] To date, different types of metal oxides have been implemented as electron mediators for ethanol sensing, such as SnO_2, WO_3, In_2O_3, Fe_2O_3, and ZnO.[13] On the other hand, bimetallic nanomaterials, such In_2O_3/ZnO nanocomposites,[14] CuO/SnO_2 nanoparticles,[15] Ga_2O_3/In_2O_3 nanocomposite,[16] SnO_2/ZnO nanostructure,[17] and TeO_2/In_2O_3 core shell nanorods,[18] have been investigated as capable and efficient ethanol-sensing materials with high sensitivity, low detection limit, large linear dynamic range, and short response time. Due to possessing an n-type wide band gap with a resistivity of 10^{-4} to 10^{12} Ω cm, ZnO is considered a key substance for selective ethanol sensing.[19] To improve the sensing performance of ZnO, semiconductors metal oxides, such as SnO_2, V_2O_5, WO_3, and MoO_3, have been investigated with ZnO as a bimetallic oxides pair.[20] Furthermore, the combination of tri-metal oxides, such as ZnO/Al_2O_3/TiO_2, $Zn_{0.4}$/$Co_{0.6}$/Al_2O_4 and ZnO/SnO_2/Ga_2O_3, have been implemented and have exhibited a better performance to sensing C_2H_5OH.[21,22]

For the purpose of environmental investigations and for application in chemical processes, many attempts have been prepared to introduce easy, simple, economical, consistent, and reliable sensors. Chemical sensors based on doped semiconductor metal oxides have many potential benefits over conventional methods, such as high response, low charge, and portability, and hence have been extensively employed for the detection of contaminated or toxic pollutants, chemical process control, and in the monitoring of air/water contamination in the environment. Ethanol is considered hazardous under medium or heavy exposure and is usually considered a serious health and environmental problem. Therefore, detection using a consistent technique with CdO/ZnO/Yb_2O_3 NSs using a GCE electrode would be desirable. The exploration of ethanol by CdO/ZnO/Yb_2O_3 NSs deposited as thin films onto GCE with a conducting binder was performed herein and then studied in detail in terms of seeking an improvement in selective and sensitive chemical sensing for environmental applications. In the methodology outlined herein, CdO/ZnO/Yb_2O_3 NSs films with conducting binders were exploited toward assessing target hazardous analytes using a trustworthy *I–V* method. It was established that the fabricated ethanol sensor was exceptional for ultra-sensitive recognition with active CdO/ZnO/Yb_2O_3 NSs onto GCE in a short response time.

Experimental

Materials and methods

The analytical grade chemical reagents, such as ammonium hydroxide, Nafion (5% ethanoic solution), 2-nitrophenol, 3-methoxyphenol, 4-aminophenol, 4-methoxyphenol, bisphenol A, ethanol, hydrazine, methanol, 1,2-dichlorobenzene, *p*-nitrophenol, monosodium phosphate, and disodium phosphate, were procured from Sigma-Aldrich, and used without any additional purification. Modern and highly reliable equipment, namely a Thermo Scientific NICOLET iS50 FTIR spectrometer (Madison, WI, USA) and 300 UV/Visible spectrophotometer (Thermo Scientific), were utilized to record the FTIR and UV/Vis spectra of the CdO/ZnO/Yb_2O_3 NSs. XPS investigations were performed on the CdO/ZnO/Yb_2O_3 NSs to determine the binding energies (eV) among Cd, Zn, Yb, and O, on a K-α1 spectrometer (Thermo Scientific, K-α1 1066) with an excitation radiation source (A1 Kα1, beam spot size = 300.0 μm, pass energy = 200.0 eV, pressure ~ 10^{-8} Torr). The optical characterizations, such as molecular arrangement, elemental analysis, morphology, and particle size of the CdO/ZnO/Yb_2O_3 NSs, were inspected using an FESEM instrument (JEOL, JSM-7600F, Japan) equipped with XEDS. In order to analyze the crystallinity of the CdO/ZnO/Yb_2O_3 NSs, the XRD assessment was conducted under ambient conditions. The ethanol sensor based on CdO/ZnO/Yb_2O_3 NSs/GCE was utilized to detect ethanol at a selective potential using a Keithley electrometer (6517A, USA) with electrochemical approaches (*i.e.*, the *I–V* method).

Preparation of CdO/ZnO/Yb_2O_3 NSs by the hydrothermal process

Cadmium chloride ($CdCl_2$), zinc chloride ($ZnCl_2$), ytterbium chloride ($YbCl_3$), and ammonium hydroxide (NH_4OH) were used as reacting precursors to prepare CdO/ZnO/Yb_2O_3 NSs by implementing the hydrothermal process. The hydrothermal method is a typical solid-state system that is widely applied in the preparation of doped nanomaterials, and results in nanomaterials that are smaller, with grain sizes reasonably smaller than those resulting from phase formation. Following this methodology, $CdCl_2$, $ZnCl_2$, and $YbCl_3$ were dissolved in distilled water (100.0 mL) in a conical flask (250.0 mL) under continuous stirring. The pH of the obtained solution was adjusted to 10.5 by adding NH_4OH, and after that, the whole solution was placed in an oven at 150.0 °C with a continuous magnetic stirring system. Finally, the produced NSs were placed in the muffle furnace for calcination at 500 °C for around 6 h. Then, the calcined sample was characterized using FTIR, UV, XRD, XPS, and FESEM.

$$NH_4OH_{(s)} \rightarrow NH_{4(aq)}^{+} + OH_{(aq)}^{-} \quad \text{(i)}$$

$$ZnCl_2 \rightarrow Zn_{(aq)}^{2+} + 2Cl_{(aq)}^{-} \quad \text{(ii)}$$

$$CdCl_2 \rightarrow Cd_{(aq)}^{2+} + 2Cl_{(aq)}^{-} \quad \text{(iii)}$$

$$YbCl_3 \rightarrow Yb_{(aq)}^{3+} + 3Cl_{(aq)}^{-} \quad \text{(iv)}$$

$$NH_{4(aq)}^{+} + 7OH_{(aq)}^{-} + Zn_{(aq)}^{2+} + Cd_{(aq)}^{2+} + Yb_{(aq)}^{3+} + Cl_{(aq)}^{-} \rightarrow Zn(OH)_{2(aq)}\downarrow + Cd(OH)_{2(aq)}\downarrow + Yb(OH)_{3(aq)}\downarrow + NH_4Cl_{(aq)} \quad \text{(v)}$$

$$Zn(OH)_{2(aq)}\downarrow + Cd(OH)_{2(aq)}\downarrow + 2Yb(OH)_{3(aq)}\downarrow \rightarrow CdO/ZnO/Yb_2O_{3(s)}\downarrow + 5H_2O_{(aq)} \quad \text{(vi)}$$

The reactions progressed slowly from (i) to (vi) above. During the preparation of the ternary metal oxides, $CdO/ZnO/Yb_2O_3$ NSs, the pH value of the reaction medium plays an important role. At a specified pH, $ZnCl_2$ is hydrolyzed in alkaline solution (ammonium hydroxide) to form zinc hydroxide rapidly, according to eqn (v). Therefore, NH_4OH was used to regulate the pH value (alkaline phase) as well as to deliver the hydroxyl ions (OH^-) slowly into the reaction medium. When the concentration of Zn^{2+} and OH^- ions are close to the critical value, nuclei formation starts in the $Zn(OH)_2$ solution. At a high concentration of Yb^{3+} and Cd^{2+} ions [reactions (iii)–(v)], the nucleation of soluble $Zn(OH)_2$ crystals become slower, because of the lower activation energy of $Zn(OH)_2$ to form heterogeneous nucleation with other oxides, such as $Cd(OH)_2$, $Zn(OH)_2$, or $Yb(OH)_3$. Due to the higher concentration of Yb^{3+} and Cd^{2+} in the reaction system, a number of larger $Cd(OH)_2$/$Zn(OH)_2$/$Yb(OH)_3$ crystals are initiated to form insoluble aggregates with a sheet-like morphology according to the reactions (v) to (vi). Then, the resultant crystals were washed thoroughly with acetone, ethanol, and water successively and kept for drying at room temperature. Finally, the doped insoluble $Cd(OH)_2$/$Zn(OH)_2$/$Yb(OH)_3$ nanocrystals were calcined at 500.0 °C for 6 h in the furnace (Barnstead Thermolyne, 6000 Furnace, USA). According to the Ostwald-ripening method for nanoparticles growth mechanism, at the very beginning, $CdO/ZnO/Yb_2O_3$ NSs nucleus are progressed by self and mutual-aggregation and then are again re-aggregated to form $CdO/ZnO/Yb_2O_3$ NSs. The inside molecular arrangement of nanocrystals are with each other's counterparts through van der Waals forces. The growth pattern of ZnO/SnO_2/Yb_2O_3 NPs are similar with the previously published reports.[23,24] The formation mechanism of the $CdO/ZnO/Yb_2O_3$ NSs are presented in Scheme 1. To the best of our knowledge, this is the first time that the produced calcined $CdO/ZnO/Yb_2O_3$ NSs have been applied to the selective detection of ethanol and consequently, there are no other reports available on this point.

Fabrication of GCE with $CdO/ZnO/Yb_2O_3$ NSs

0.1 M phosphate buffer (PBS solution) at pH 7.0 was prepared by mixing an equi-molar concentration of 0.2 M Na_2HPO_4 and 0.2 M NaH_2PO_4 solution in 100 mL de-ionized water at room temperature. A thin layer of prepared NSs was deposited onto a GCE with conducting binder (5% ethanolic Nafion solution) to result in a working electrode as an ethanol sensor. Then, it was kept in the oven at 35 °C, until the film was completely dried, stable, and smooth. An electrochemical cell was assembled with $CdO/ZnO/Yb_2O_3$ NSs/binders/GCE and Pt-wire (dia., 1.5 mm) as the working and counter electrodes, respectively. Ethanol was diluted to make various concentrations (full concentration range: 0.35 nM to 0.35 M) in de-ionized water and used as a target analyte. The ratio of the current *versus* concentration (the slope of the calibration curve) was used to calculate the working electrode sensitivity. Detection limit was evaluated from the ratio of 3N/S (ratio of noise × 3 *vs.* sensitivity) from the linear dynamic range of the calibration curve. The utilized electrometer for the current *vs.* potential (*I–V*) measurements was a simple two-electrode system. The amount of 0.1 M PBS solution was kept constant in the beaker as 10.0 mL throughout the chemical investigation.

Results and discussions

Optical and structural analyses

The optical property of $CdO/ZnO/Yb_2O_3$ NSs is one of the most important characteristics to the assessment of its photocatalytic activity. Based on the visible light principle (UV-vis) theory, the outer electron of the atom absorbs radiant energy at a desired wavelength and it is then transited from a lower to a higher energy level to result in a UV-vis spectrum, which is illustrated in Fig. 1a. UV-vis spectroscopy is performed in the range of 400 nm to 800 nm at room temperature. The observed spectrum shows an intense, identical and wide spectrum at 307 nm, which is represented the electronic transition of the valence band of $CdO/ZnO/Yb_2O_3$ NSs from lower to higher energy level. According to eqn (vii), the calculated band gap energy (E_{bg}) is 4.04 eV at the point of the highest absorption band of $CdO/ZnO/Yb_2O_3$.[25]

$$E_{bg}\ (\text{eV}) = \frac{1240}{\lambda} \quad \text{(vii)}$$

where, E_{bg} = band gap energy and λ = maximum absorbed wavelength.

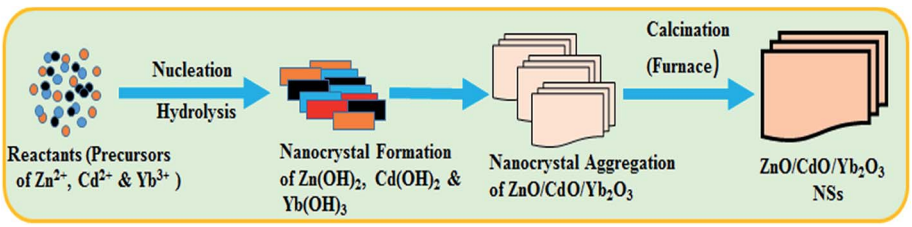

Scheme 1 Schematic of the growth mechanism of $CdO/ZnO/Yb_2O_3$ NSs by a facile hydrothermal process.

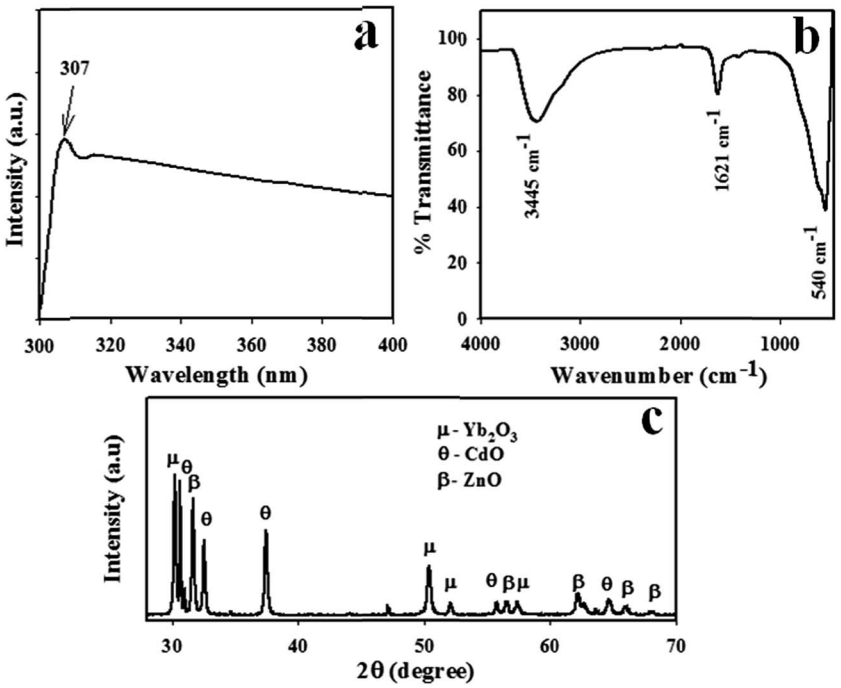

Fig. 1 Optical and morphological evaluation by (a) UV spectrum, (b) FTIR, and (c) XRD pattern of the $CdO/ZnO/Yb_2O_3$ NSs.

FTIR is a modern analysis tool, which can be used to determine the functional properties of an atom or molecule from the corresponding atomic and molecular vibrations. Therefore, the synthesized NSs of $CdO/ZnO/Yb_2O_3$ were investigated by FTIR analysis. FTIR was performed in the region of 450–4000 cm^{-1}, as demonstrated in Fig. 1b. According to the FTIR spectrum, the observed major peaks could be detected at 3445, 1621, and 540 cm^{-1}, respectively. The peaks at 3445 and 1621 cm^{-1} are associated with the standard OH stretching and H_2O bending modes correspondingly. The peak at 540 cm^{-1} peak is connected to the stretching of Cd–O or Zn–O.[26,27] X-ray powder diffraction (XRD) is one of the standard analytical techniques and is widely used for phase identification of a crystalline nanomaterial and it can also convey information about a unit cell's dimensions. For exploration of the structural properties and crystal phase of the synthesized $CdO/ZnO/Yb_2O_3$ NSs, powder X-ray diffraction (XRD) was performed with Cu–K1 radiation (=1.54178 Å) in the range of 10–80° with a 2° min^{-1} scanning speed. The observed XRD pattern exhibited that the NSs were well crystalline in nature and had mixed phases of CdO, ZnO, and Yb_2O_3, as shown in Fig. 1c. The apparent diffraction reflections of the ZnO indices as β were (100), (110), (103), (024), (112), and (200), which are similar to bulk ZnO and the hexagonal phase of ZnO.[28] The observed reports share great similarities with the standard JCPDS data card (JCPDS no. 36-1451). The other several peaks of the CdO indices as θ were (111), (200) and (220), which are well matched with the literature.[29] Besides this, some other sharp peaks of Yb_2O_3 indices as μ were also observed in the XRD diffraction pattern, which were indicated as (101), (110), (112), and (200) and completely agreed with the reported literature.[30,31] Moreover, the sharpness of the peaks showed that the product NSs were well crystallized.

Morphological and elemental analysis

FESEM investigation was carried out for the morphological studies of the synthesized $CdO/ZnO/Yb_2O_3$ NSs, and the resultant representative low and high magnifying images of FESEM are presented in Fig. 2a and b. These clearly show uniform and aligned $CdO/ZnO/Yb_2O_3$ nanosheets.[32] The X-ray energy-dispersive spectroscopy (EDS) exploration of $CdO/ZnO/Yb_2O_3$ NSs indicated the existence of Cd, Zn, Yb, and O arrangements in the pure calcined doped nanosheet materials, and clearly displayed that the calcined prepared materials are organized with only cadmium, zinc, ytterbium, and oxygen elements, which is illustrated in Fig. 2c and d. The composition of Cd, Zn, Yb, and O are 4.51%, 9.03%, 65.03%, and 21.43%, correspondingly. No other peaks connected with any impurity were apparent in the EDS, which supports that the $CdO/ZnO/Yb_2O_3$ NSs products contain only Cd, Zn, Yb, and O.[25]

XPS analysis

To the advance evidence for the conformation of components existing in the prepared sample $CdO/ZnO/Yb_2O_3$ NSs, the quantitative spectroscopic technique XPS was implemented on the NSs. The chemical nature of the elements present and the kinetic energy, including the number of electrons existing in the sample during X-ray beam irradiation of, can be expected by the implication of XPS inspection.[33] The high resolution XPS spectra of O 1s, Cd 3p, Zn 2p, and Yb 4d are demonstrated in Fig. 3. Regarding the main two identical peaks of Cd 3d orbit, there is no apparently change between these two peaks, with both peaks being an indication of the equal oxidation state of Cd. The binding energies of Cd $3d_{5/2}$ and Cd $3d_{3/2}$ are 406.08 eV and 414.08 eV, respectively, which are the characteristic values

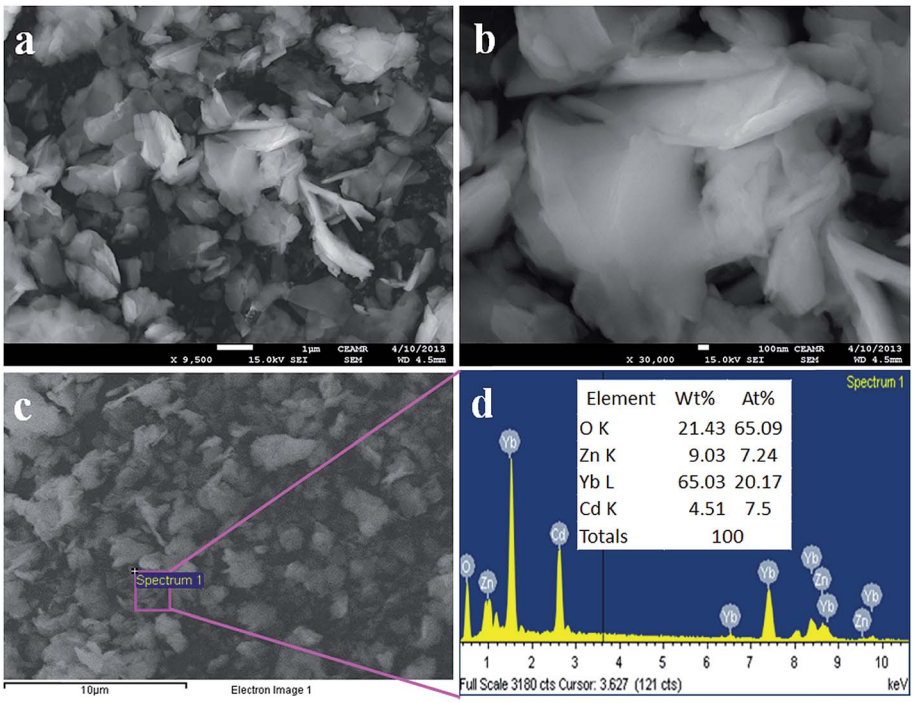

Fig. 2 (a and b) FESEM analysis from low to high magnified images, and (c and d) elemental analysis of CdO/ZnO/Yb_2O_3 NSs.

of Cd^{2+} in CdO, as illustrated in Fig. 3c. The O 1s, in Fig. 3b, is broad and asymmetric, indicating the presence of multi-component oxygen species.[34] In Fig. 3d, the observed binding energy of Zn $2p_{3/2}$ and Zn $2p_{1/2}$ peaks are 1023.08 and 1046.08 eV, correspondingly, which are the characteristic values for the oxidation of Zn^{2+} in ZnO.[35] Furthermore, the noticeable

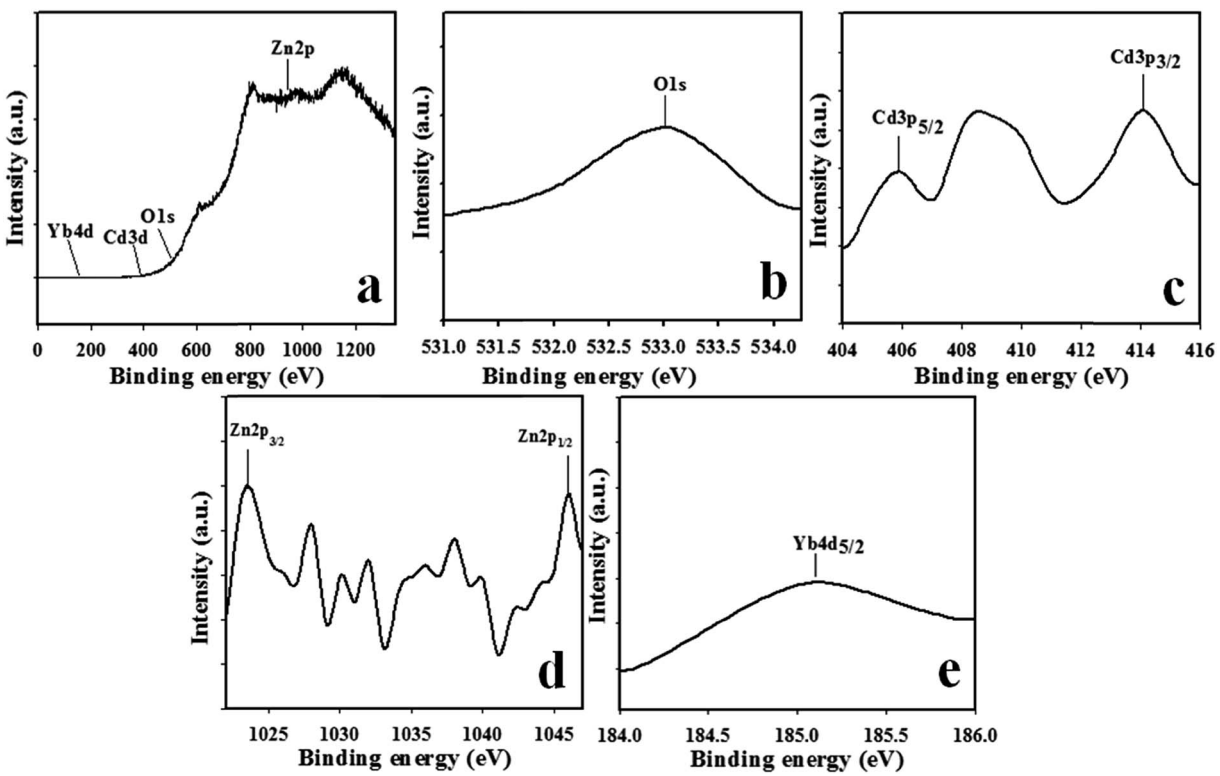

Fig. 3 Binding energy analysis by XPS study of the CdO/ZnO/Yb_2O_3 NSs: (a) full spectrum, (b) O 1s, (c) spin orbit Cd 3p level, (d) spin orbit Zn 2p level, and (e) spin orbit Yb 4d level.

peak of the Yb 4d spectrum in Fig. 3e is positioned at 185.08 eV, which can be accredited to Yb $4d_{5/2}$, which is in good agreement with the Yb 4d binding energy of Yb_2O_3.[36,37]

Applications

Detection of ethanol with CdO/ZnO/Yb_2O_3 NS materials

The possible implementation of the CdO/ZnO/Yb_2O_3 NSs/Nafion/GCE combination as a chemical sensor (selective to ethanol) was performed for measuring and detecting target chemicals in a buffer system. The enrichment of CdO/ZnO/Yb_2O_3 NSs/Nafion/GCE as chemical sensors is in the initial stages of development and consequently no other reports are available in the literature. The CdO/ZnO/Yb_2O_3 NSs/Nafion/GCE sensor has a number of advantages, such as stability in air, non-toxicity, chemical inertness, electrochemical activity, simplicity to assemble, ease in fabrication, and chemo-safe characteristics. The feasible application of CdO/ZnO/Yb_2O_3 NSs onto a GCE as a chemical sensor was assessed in detail. The synthesized NSs were used as an effective electron mediator for construction of the ethanol chemical sensor. To fabricate the highly selective ethanol chemical sensor, a thin layer of prepared NSs was deposited onto GCE and then dried at room temperature. For the improvement of the conducting binding properties between NSs and GCE, a drop of Nafion (5% ethanolic Nafion solution) was added. The modified GCE was placed into an oven at low temperature for 2 h to make it smooth, dry, stable, and a uniform surface. Consequently, the fabricated CdO/ZnO/Yb_2O_3 NSs/Nafion/GCE was tested as a working electrode in the construction of a chemical sensor to detect ethanol. During the sensing performance of ethanol, the applied current *vs.* potential (*I*–*V*) was assessed on a thin film of CdO/ZnO/Yb_2O_3 NSs/Nafion/GCE (working electrode), and it was found to increase remarkably due to the adsorption of aqueous ethanol on the fabricated working electrode. The holding period of the electrometer was set at 1.0 s. When the alcohol was exposed to the surface oxygen ions of the CdO/ZnO/Yb_2O_3 NSs, it reacted with either O^- or O^{2-} ions and was oxidized to carbon dioxide and water and released electrons, which essentially increased the conductivity of the buffer medium. Additionally, it is known that the sensing capacity is related to the grain size of the nanomaterials of CdO/ZnO/Yb_2O_3. Since the proposed ethanol sensor exhibited a relatively higher sensitivity, it could be predicted that the produced NSs had a small grain size, high specific surface area, and high surface atomic activity. Therefore, the ethanol sensor based on CdO/ZnO/Yb_2O_3 NSs demonstrated a greater response to ethanol and higher sensitivity than the other tested composites.[38] The fabricated-surface of the CdO/ZnO/Yb_2O_3 NSs sensor was prepared with conducting binders on the GCE surface, as presented in Scheme 2a. The theoretical *I*–*V* signals of the chemical sensor with the doped thin film were estimated as a function of current *vs.* potential for ethanol and are presented in Scheme 2b. The electrical responses to the target ethanol were investigated by a simple and reliable *I*–*V* technique using the CdO/ZnO/Yb_2O_3 NSs-fabricated GCE film, which is presented in Scheme 2c. A considerable amplification in the current response with the applied potential was perceptibly confirmed. The simple, reliable, possible reaction mechanism is generalized in Scheme 2 in the presence of ethanol on the CdO/ZnO/Yb_2O_3 NSs surfaces by the *I*–*V* method. The ethanol is converted to water and carbon dioxide in the presence of the doped semiconductor nanomaterials by releasing electrons ($6e^-$) to the reaction system from the conduction band (C.B.) of the prepared NSs, which improved and enhanced the current responses against the potential during the *I*–*V* measurement at room temperature.

The modified GCE was not equally active in all buffer media. Therefore, it was investigated in various buffer systems (pH of 5.7, 6.5, 7.0, 7.5, and 8.0) and it was found that at pH 7.0, the fabricated working electrode had the maximum responsive, as

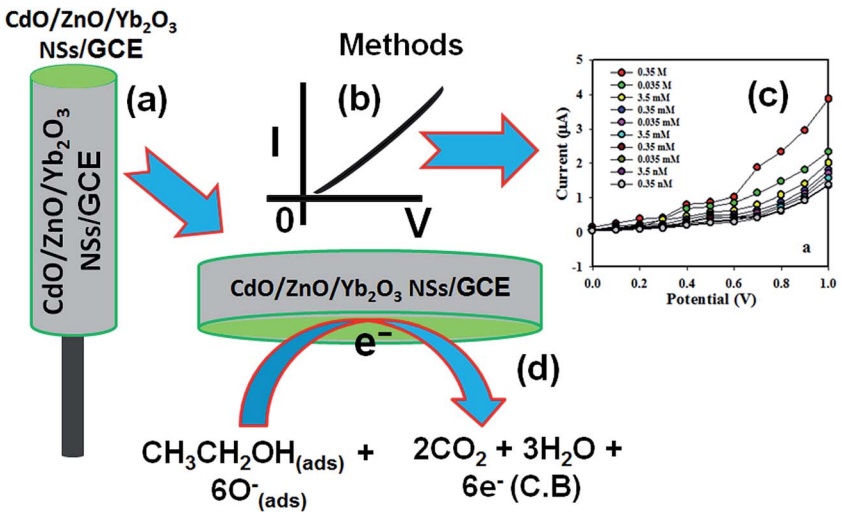

Scheme 2 Schematic of: (a) the fabricated CdO/ZnO/Yb_2O_3 NSs with conducting binders (5% Nafion), (b) *I*–*V* detection methodology (theoretical), (c) outcomes of the *I*–*V* experimental result, and (d) the reaction mechanism of ethanol in the presence of the semiconductor CdO/ZnO/Yb_2O_3 NSs.

illustrated in Fig. 4a. *I–V* measurements using the Keithley electrometer were carried out at the applied potential range of 0 to +1.5 V. Various toxins, such as 2-nitrophenol, 3-methoxyphenol, 4-aminophenol, 4-methoxyphenol, bisphenol A, methanol, ethanol, ammonium hydroxide, 1,2-dichlorobenzene, and *p*-nitrophenol were applied to study the selectivity of the sensor. Based on the selectivity study, ethanol exhibited the maximum current response toward the CdO/ZnO/Yb_2O_3 NSs/GCE electrode, as presented in Fig. 4b, where the applied potential range of the *I–V* measurement was 0 to +1.0 V. Additional selectivity was also studied in the presence of common alcohols, such as ethanol, methanol, butanol, and propanol, and the results are presented in the ESI (Fig. S1; Ψ),† the reproducibility study of the fabricated GCE based on CdO/ZnO/Yb_2O_3 NSs was performed at 0.1 μM concentration of ethanol solution in the desire buffer medium, as presented in Fig. 4c. Intra-day and inter-day repeatability were tested and included in the ESI (Fig. S2; Ω and S3; η).† Outstanding reproducible responses were obtained under similar conditions and it was found that the *I–V* responses did not change after washing the fabricated electrode in each trial. The calculated standard deviation of reproducibility (RSD) was 2.27% at a potential +0.5 V. The response time is another tool for the measurement of efficiency of the fabricated CdO/ZnO/Yb_2O_3 NSs/GCE, whereby the test was executed in 0.1 μM ethanol solution and the observed response time was 9.2 s, as illustrated in Fig. 4d. During this performance, the sensing current was measured with respect to time and it was observed that after 9.2 s, the sensing current was almost steady. The variation in the sensing current response on the modified GCE with the CdO/ZnO/Yb_2O_3 NSs is a function of the concentration of ethanol. Therefore, the *I–V* responses of the modified CdO/ZnO/Yb_2O_3 NSs/GCE sensor were examined with different concentrations of ethanol and it was found they were amplified with the increasing concentration of the electrolyte (ethanol) in the buffer medium.

To compute the performance of the ethanol chemical sensor, the linearity (r^2: 0.9845) of the calibration plot was found at +1.0 V over the concentration range of 0.35 nM to 3.5 mM from the lower-higher concentration of ethanol solution, as shown in Fig. 5a. The sensitivity (7.4367 μA mM^{-1} cm^{-2}) of the fabricated electrode was calculated from the ratio of the curve (current *versus* concentration ratio). The linear dynamic ranges (LDR: 0.35 nM to 3.5 mM) and detection limit (LoD: 0.127 ± 0.006 nM & LoQ: 0.423 nM) were calculated from calibration curve at a signal-to-noise ratio of 3.

In the two-electrode system (working and counter electrode), the *I–V* characteristic of the CdO/ZnO/Yb_2O_3 NSs/GCE was activated as a function of ethanol concentration in the desired buffer system, where an enhanced current response could be perceived. As observed, the response of the current increased with the increasing concentration of ethanol, and conversely an analogous phenomenon for toxic chemical detection has also

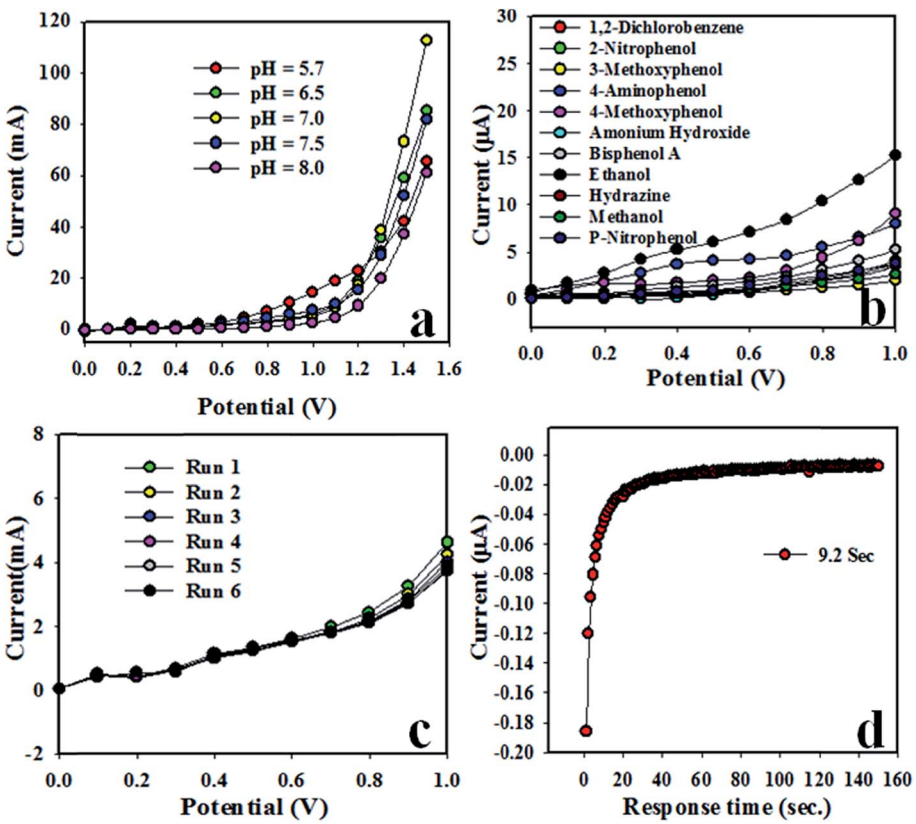

Fig. 4 Optimization of the ethanol sensor with CdO/ZnO/Yb_2O_3 NSs/GCE: (a) pH optimization, (b) selectivity, (c) repeatability, and (d) response time.

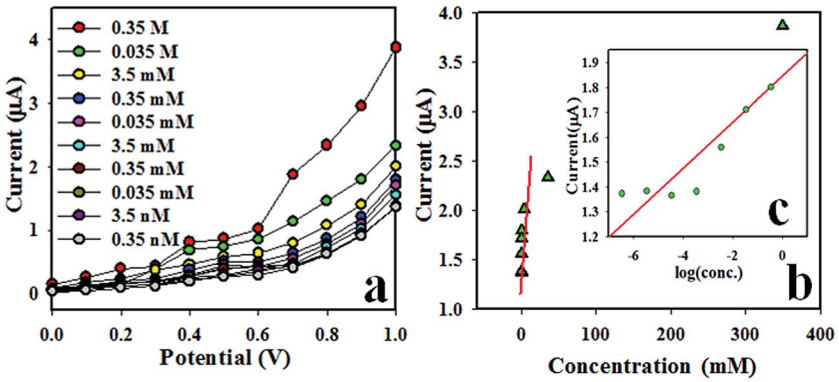

Fig. 5 (a) Concentration variation of the ethanol sensor based on CdO/ZnO/Yb_2O_3 NSs/GCE by the *I–V* method and (b) calibration curve (inset: log[EtOH·Conc.] *vs.* current).

been reported earlier.[39–42] At a very low concentration of ethanol in the measuring buffer medium, there is a smaller surface coverage of ethanol molecules on the CdO/ZnO/Yb_2O_3 NSs/GCE film. With enrichment of the ethanol concentration, the surface reaction is gradually increased (which gradually increases the response as well) owing to a larger surface area contacted with the ethanol molecules. Again, with a greater increase in ethanol concentration on the CdO/ZnO/Yb_2O_3 NSs/GCE surface, a more rapid increase in the current response was shown, due to the larger surface covered by ethanol. Then, with an additional enrichment of ethanol concentration, the surface coverage of ethanol molecules on CdO/ZnO/Yb_2O_3 NSs/GCE surface reaches saturation. Therefore, it can be summarized that the proposed ethanol chemical sensor based on the CdO/ZnO/Yb_2O_3 NSs/GCE assembly could be engaged for the successive detection and quantification of the targeted toxin (ethanol). As we observed, the proposed ethanol sensor showed a very short response time at around 10 s, where it should be mentioned that the 10 s is needed by the desire ethanol chemical sensor based on ZnO/SnO_2/Yb_2O_3 NPs/GCE to reach steady state saturation. The higher sensitivity of the modified CdO/ZnO/Yb_2O_3 NSs/GCE assembly can be accredited to the outstanding absorption ability and high catalytic-decomposition activity.[1,38,43–45] The projected sensitivity of the CdO/ZnO/Yb_2O_3 NSs/GCE sensor is comparatively higher and the detection limit is reasonably lower than earlier reported ethanol sensors based on other nanomaterials-modified electrodes according to *I–V* systems. The high sensitivity of the CdO/ZnO/Yb_2O_3 NSs/GCE delivers high electron communication features, which includes enhanced direct electron transfer between the active sites of CdO/ZnO/Yb_2O_3 NSs/GCE and the analyte (ethanol). The CdO/ZnO/Yb_2O_3 NSs/GCE system was thus demonstrated as a simple and reliable route for the detection of ethanol using GCE-electrodes. It also revealed significant access to a large group of chemicals for a wide range of environmental applications in environmental and health-care fields, respectively. The sensing performance of the earlier testified metal oxides-based ethanol sensors are summarized in Table 1 in terms of sensitivity, detection limit (LoD), and linear dynamic range (LDR).[1,45–51] It should be noted that the proposed ethanol sensor based on CdO/ZnO/Yb_2O_3 NSs exhibited better sensing performance, particularly in terms of sensitivity, LoD and LDR.

In general, at room temperature, the resistance value of the doped sensors decrease with the increasing working potential due to the fundamental characteristics of the semiconductor-doped nanomaterials.[52] Actually, oxygen adsorption demonstrates an important responsibility in the electrical properties of the CdO/ZnO/Yb_2O_3 with nanosheets structures. Oxygen ion adsorption removes the conduction of electrons and increases the resistance of the CdO/ZnO/Yb_2O_3 NSs. Oxygen species such as O_2^- and O^- are adsorbed on the doped material surface at calcination temperature, where the quantity of such chemisorbed oxygen species depend on the structural properties. At room conditions, O_2^- is chemisorbed, while in a nanosheets

Table 1 Performances of typical electrochemical sensing materials for ethanol detection

Modified electrode	LoD	LDR	Sensitivity	Ref.
Ni doped SnO_2	0.6 nM	1.0 nM to 1.0 mM	2.3148 μA mM^{-1} cm^{-2}	1
ZnO/CuO NSs	10.65 nM	1.7 mM to 1.7 M	2.1949 μA mM^{-1} cm^{-2}	45
CeO_2 NMs	0.124 mM	0.17 mM to 0.17 M	0.9200 μA mM^{-1} cm^{-2}	46
CuO NSs	0.14 mM	0.17 mM to 1.7 M	0.9722 μA μM^{-1} cm^{-2}	47
CuO–Fe_2O_3 nanocubes	0.08 mM	0.1 nM to 0.1 mM	7.258 μA mM^{-1} cm^{-2}	48
Sm–Co_3O_4 nanokernels	0.63 nM	1.0 nM to 10.0 mM	2.1991 μA mM^{-1} cm^{-2}	49
Gd_2O_3 nanorods	0.02 mM	0.17 mM to 0.85 M	0.6940 μA mM^{-1} cm^{-2}	50
Nanohybrid PPC/silica materials	20.70 μM	0.17 mM to 0.85 M	0.5698 μA mM^{-1} cm^{-2}	51
CdO/ZnO/Yb_2O_3 NSs	**0.127 ± 0.006 nM**	**0.35 nM to 3.5 mM**	**7.4367 μA mM^{-1} cm^{-2}**	**This work**

morphology, O_2^- and O^- are chemisorbed, and the O_2^- disappears rapidly.[53] Here, the ethanol-sensing mechanism of the CdO/ZnO/Yb_2O_3 NSs sensor is based on semiconductors oxides, due to the oxidation or reduction of the semiconductor oxide nanosheets, according to the dissolved O_2 in bulk-solution or surface-air of the neighboring atmosphere according to the eqn (viii) and (ix):

$$e^-(CdO/ZnO/Yb_2O_3NSs) + O_2 \rightarrow O_2^- \quad \text{(viii)}$$

$$e^-(CdO/ZnO/Yb_2O_3NSs) + O_2^- \rightarrow 2O^- \quad \text{(ix)}$$

These reactions are attained in a bulk-system or air/liquid interface or adjacent atmosphere owing to the small carrier concentration, which improves the resistance. The ethanol sensitivity toward CdO/ZnO/Yb_2O_3 NSs (*e.g.*, MO_x) could be attributed to the high oxygen deficiency and imperfection density effects to increasing the oxygen adsorption. The larger the quantity of oxygen adsorbed on the sensor surface, the larger would be the oxidizing potential and the faster would be the oxidation of ethanol. The reactivity of ethanol was very high as compared to that of other chemical towards the surface under similar condition.[54–56] When ethanol reacts with the adsorbed oxygen on the exterior/interior of the layer, it oxidized to carbon dioxide and water, releasing free electrons ($6e^-$) in the conduction band, which could be expressed through the following reaction (x):

$$CH_3CH_2OH_{(ads)} + 6O_{(ads)}^- \rightarrow 2CO_2 + 3H_2O + 6e^-(C.B.) \quad \text{(x)}$$

In the reaction medium, these reactions referred to oxidation of the reducing carriers. These methods improved the carrier concentration and consequently decreased the resistance on contact to the reducing liquids/analytes. Under room conditions, the exposure of a metal oxide surface to reducing liquid/analytes results in a surface-mediated incineration procedure. The abolition of ionosorbed oxygen amplifies the electron concentration and hence the surface conductance of the film.[57] The reducing analyte (ethanol) provides electrons to the CdO/ZnO/Yb_2O_3 NSs surface. Consequently, resistance is reduced, and hence the conductance is increased. This is the reason why the analyte response (current) is amplified with the escalating potential. Thus, the produced electrons contribute to a rapid increase in conductance of the thick film. The CdO/ZnO/Yb_2O_3 NSs unusual regions dispersed on the surface progress the capability of the material to absorb more oxygen species, giving high resistance in ambient air, as presented in Scheme 3.

The high ethanol response of the CdO/ZnO/Yb_2O_3 NSs was investigated in more detail relative to the probable chemical-sensing mechanism. It is a p-type semiconductor nanomaterial. The oxide surface of a p-type semiconductor is readily covered with chemisorbed oxygen.[58] Therefore, at the sensing condition, the adsorption of negatively charged oxygen can generate the holes for conduction. The subsequent ethanol-sensing reactions might be considered according to the charges of the adsorbed oxygen species under the statement of full oxidation of C_2H_5OH according to the following eqn (xi) and (xii):

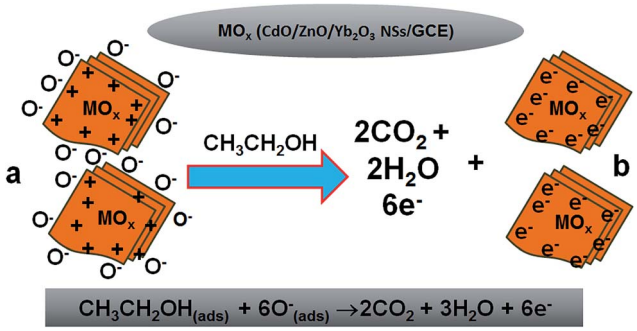

Scheme 3 Mechanism of CdO/ZnO/Yb_2O_3 NSs ethanol sensors under ambient conditions: (a) before ethanol injection and (b) after ethanol addition.

$$\tfrac{1}{2}O_{2(g/l)} \rightarrow O_{(ads)}^- + h^\circ \quad \text{(xi)}$$

$$C_2H_5OH_{(g)} + 6O_{(ads)}^- + 6h^\circ \rightarrow 2CO_{2(g)} + 3H_2O_{(g)} \quad \text{(xii)}$$

That is, the oxidation reaction with reducing ethanol amplifies the resistivity of the surface regions of the p-type CdO/ZnO/Yb_2O_3 NSs, which in turn enhances the sensor resistance. The resistive contacts among the nanomaterials control the chemi-sensor resistance. Accordingly, the ethanol response is significantly dependent upon the dimensions of the nano-kernels, the large active surface area, and the nanoporosity. According to the charge accumulation reproduction of p-type semiconductors, the conduction occurs along the conductive as well as active sensor surface.[59–61] The conductivity of ZnO thin films doped with CdO/Yb_2O_3 is very sensitive to the exposure of the surface to various chemicals and hence it can be used as a toxic chemical sensor capable of detecting the toxicity of contaminants, due to the high sensitivity to selective chemicals present in the sensing layer.[62] Recent experiments revealed the existence of a surface electron accumulation layer in vacuum annealed single crystals, which disappears upon exposure to ambient air.[63] This layer may play a role in sensor action as well. The presence of this conducting surface channel has been suggested to be related to some puzzling type-conversion effects observed when attempting to obtain p-type co-doped CdO/Yb_2O_3 with ZnO.[64,65] Note that most of the growth techniques produce CdO/Yb_2O_3-doped ZnO that is highly p-type. This high level of p-type conductivity is very useful for chemical-sensing applications as an electro-catalyst, such as with transparent conductors, but in general, it would be desirable to have better control over the conductivity. In particular, the ability to reduce the p-type background and to achieve p-type doping would open up tremendous possibilities for semiconductor device applications, especially related to the compensation of the predominant acceptor or donor dopants, *i.e.*, donor defects are easier to form in p-type materials, whereas acceptor defects are easier to form in n-type materials, always counteracting the prevailing conductivity. Native defects have long been believed to play an even more important role in ZnO, which frequently exhibits high levels of unintentional p-type conductivity. Oxygen vacancies and zinc interstitials have often been invoked as

Table 2 Measured concentration of the ethanol analytes in real samples

Sample	Added ethanol concentration	Determined ethanol concentration[a] by CdO/ZnO/Yb_2O_3 NSs/GCE	Recovery[b] (%)	RSD[c] (%) ($n = 3$)
Industrial effluent	0.3500 μM	0.3301 μM	94.31	2.44
	0.3500 μM	0.3326 μM	95.02	
	0.3500 μM	0.3464 μM	98.97	
Plastic baby bottle	0.3500 μM	0.3302 μM	94.34	3.19
	0.3500 μM	0.3350 μM	95.71	
	0.3500 μM	0.3437 μM	98.2	
Plastic water bottle	0.3500 μM	0.3266 μM	93.31	1.08
	0.3500 μM	0.3378 μM	96.51	
	0.3500 μM	0.3411 μM	97.46	
PVC food packaging bag	0.3500 μM	0.3375 μM	96.43	0.53
	0.3500 μM	0.3481 μM	99.46	
	0.3500 μM	0.35 μM	100.00	

[a] Mean of three repeated determinations (signal-to-noise ratio of 3) with CdO/ZnO/Yb_2O_3 NSs/GCE. [b] Concentration of ethanol determined/concentration of ethanol taken. [c] Relative standard deviation value indicates precision among three repeated determinations.

sources of p-type conductivity in CdO/ZnO/Yb_2O_3.[66,67] However, most of these arguments are based on indirect evidence, *e.g.*, that the electrical conductivity increases as the oxygen partial pressure decreases. In our view, these statements about the role of native point defects as sources of conductivity are only hypotheses that are not supported by experimental observations. In fact, they are in contradiction with several careful experiments, as well as with accurate density-functional calculations. In the following, we discuss the theory of point defects in ZnO, with an emphasis on the results of density-functional calculations, and relate these to experimental observations whenever possible.[68]

Real sample analysis

To establish validation, the fabricated sensors based on CdO/ZnO/Yb_2O_3 NSs coated onto GCE were applied to detect ethanol in real samples with various concentrations of ethanol. We used these to measure ethanol in industrial effluent, plastic baby bottle, plastic water bottle, and PVC food packaging bag. The results showed us that ethanol detection is possible in environmental samples, as shown in Table 2.

Conclusions

In this study, NSs of CdO/ZnO/Yb_2O_3 were prepared by implementation of a facile hydrothermal method in alkaline medium. Then, the calcined NSs were characterized by the investigation *via* XRD, XPS, FTIR, SEM, and EDS analyses. A thin layer of CdO/ZnO/Yb_2O_3 NSs was deposited onto a GCE with conducting binder to result in a working electrode of an ethanol sensor. The invented ethanol sensor based on CdO/ZnO/Yb_2O_3 NSs/Nafion/GCE acted as an efficient electron mediator for the detection of ethanol using the *I–V* method. The key electrochemical features of the fabricated ethanol sensor were its excellent detection limit, linear dynamic range, sensitivity, repeatability, robustness, stability, and response time. The CdO/ZnO/Yb_2O_3 NSs/Nafion/GCE assembly exhibited a higher sensitivity (7.4367 μA mM^{-1} cm^{-2}), and lower detection limit (0.127 ± 0.006 nM) and limit of quantification (0.423 ± 0.02 nM) compared to previously reported chemical sensors. As exposed from the interference studies, the fabricated sensor provided high selectivity toward the detection of ethanol in the presence of other chemicals. This original attempt resulted in a well-organized reliable technique for the development of a proficient chemical sensor for application with environmental hazardous chemicals and in the biomedical health-care field.

Acknowledgements

Center of Excellence for Advanced Materials Research (CEAMR), Chemistry Department, King Abdulaziz University, Jeddah, Saudi Arabia is highly acknowledged for materials preparation and sensor development research facilities.

References

1 M. M. Rahman, A. Jamal, S. B. Khan and M. Faisal, Highly sensitive ethanol chemical sensor based on Ni-doped SnO_2 nanostructure materials, *Biosens. Bioelectron.*, 2011, **28**, 127–134.
2 M. Yu, G. Suyambrakasam, R. Wua and M. Chavali, Performance evaluation of ZnO–CuO hetero junction solid state room temperature ethanol sensor, *Mater. Res. Bull.*, 2012, **47**, 1713–1718.
3 A. Mirzaei, K. Janghorban, B. Hashemi, M. Bonyani, S. G. Leonardi and G. Neri, Highly stable and selective ethanol sensor based on α-Fe_2O_3 nanoparticles prepared by Pechini sol–gel method, *Ceram. Int.*, 2016, **42**, 6136–6144.
4 D. Zhu, Y. Fu, W. Zang, Y. Zhao, L. Xing and X. Xue, Room-temperature self-powered ethanol sensor based on the piezo-surface coupling effect of hetero structured α-Fe_2O_3/ZnO nanowires, *Mater. Lett.*, 2016, **166**, 288–291.
5 A. Mhamdi, A. Labidi, B. Souissi, M. Kahlaoui, A. Yumak, K. Boubaker, A. Amlouk and M. Amlouk, Impedance spectroscopy and sensors under ethanol vapors application

of sprayed vanadium-doped ZnO compounds, *J. Alloys Compd.*, 2015, **639**, 648–658.

6 J. Shi, P. Ci, F. Wang, H. Peng, P. Yang, L. Wang, Q. Wang and P. K. Chu, Pd/Ni/Si-microchannel-plate-based amperometric sensor for ethanol detection, *Electrochim. Acta*, 2011, **56**, 4197–4202.

7 S. Ameen, M. S. Akhtar and H. S. Shin, Highly sensitive hydrazine chemical sensor fabricated by modified electrode of vertically aligned zinc oxide nanorods, *Talanta*, 2012, **100**, 377–383.

8 R. Ahmad, N. Tripathy, D. Jung and Y. B. Hahn, Highly sensitive hydrazine chemical sensor based on ZnO nanorods field-effect transistor, *Chem. Commun.*, 2014, **50**, 1890–1893.

9 T. Zhoua, P. Lu, Z. Zhanga, Q. Wang and A. Umar, Perforated Co_3O_4 nanoneedles assembled in chrysanthemum-like Co_3O_4 structures for ultra-high sensitive hydrazine chemical sensor, *Sens. Actuators, B*, 2016, **235**, 457–465.

10 L. Mei, J. Deng, X. Yin, M. Zhang, Q. Li, E. Zhang, Z. Xu, L. Chen and T. Wang, Ultrasensitive ethanol sensor based on 3D aloe-like SnO_2, *Sens. Actuators, B*, 2012, **166**, 7–11.

11 M. Parthibavarman, B. Renganathan and D. Sastikumar, Development of high sensitivity ethanol gas sensor based on Co-doped SnO_2 nanoparticles by microwave irradiation technique, *Curr. Appl. Phys.*, 2013, **13**, 1537–1544.

12 F. S. Husairi, J. Rouhi, K. A. Eswar, C. H. R. Ooi, M. Rusop and S. Abdullah, Ethanol solution sensor based on ZnO/PSi nanostructures synthesized by catalytic immersion method at different molar ratio concentrations: An electrochemical impedance analysis, *Sens. Actuators, A*, 2015, **236**, 11–18.

13 E. Wongrat, N. Chanlek, C. Chueaiarrom, B. Samransuksamer, N. Hongsitha and S. Choopun, Low temperature ethanol response enhancement of ZnO nanostructures sensor decorated with gold nanoparticles exposed to UV illumination, *Sens. Actuators, A*, 2016, **251**, 188–197.

14 M. Gholami, A. A. Khodadadi, A. A. Firooz and Y. Mortazavi, In_2O_3–ZnO nanocomposites: High sensor response and selectivity to ethanol, *Sens. Actuators, B*, 2015, **212**, 395–403.

15 R. N. Mariammal, K. Ramachandran, B. Renganathan and D. Sastikumar, On the enhancement of ethanol sensing by CuO modified SnO_2 nanoparticles using fiber-optic sensor, *Sens. Actuators, B*, 2012, **169**, 199–207.

16 M. Bagheri, A. A. Khodadadi, A. R. Mahjoub and Y. Mortazavi, Strong effects of gallia on structure and selective responses of Ga_2O_3–In_2O_3 nanocomposite sensors to either ethanol, CO or CH_4, *Sens. Actuators, B*, 2015, **220**, 590–599.

17 F. A. Harraz, A. A. Ismail, A. A. Ibrahim, S. A. Al-Sayari and S. A. Al-Assiri, Highly sensitive ethanol chemical sensor based on nanostructured SnO_2 doped ZnO modified glassy carbon electrode, *Chem. Phys. Lett.*, 2015, **639**, 238–242.

18 H. Ko, S. Park, S. An and C. Lee, Enhanced ethanol sensing properties of TeO_2/In_2O_3 core shell nanorod sensors, *Curr. Appl. Phys.*, 2013, **13**, 919–924.

19 E. Wongrat, N. Chanlek, C. Chueaiarrom, B. Samransuksamer, N. Hongsitha and S. Choopun, Low temperature ethanol response enhancement of ZnO nanostructures sensor decorated with gold nanoparticles exposed to UV illumination, *Sens. Actuators, A*, 2016, **251**, 188–197.

20 S. Yang, Y. Liu, T. Chen, W. Jin, T. Yang, M. Cao, S. Liu, J. Zhou, G. S. Zakharov and W. Chen, Zn doped MoO_3 nanobelts and the enhanced gas sensing properties to ethanol, *Appl. Surf. Sci.*, 2017, **393**, 377–384.

21 S. D. Kapse, F. C. Raghuwanshi, V. D. Kapse and D. R. Patil, Characteristics of high sensitivity ethanol gas sensors based on nanostructured spinel $Zn_{1-x}Co_xAl_2O_4$, *Curr. Appl. Phys.*, 2012, **12**, 307–312.

22 L. Yu, S. Liu, B. Yang, J. Wei, M. Lei and X. Fan, Sn–Ga co-doped ZnO nanobelts fabricated by thermal evaporation and application to ethanol gas sensors, *Mater. Lett.*, 2015, **141**, 79–82.

23 S. J. Young, Y. H. Liu, C. H. Hsiao, S. J. Chang, B. C. Wang, T. H. Kao, K. S. Tsai and S. L. Wu, ZnO-Based ultraviolet photodetectors with novel nanosheet structures, *IEEE Trans. Nanotechnol.*, 2014, **13**, 238–244.

24 R. Zhang, M. Hummelgard and H. Olin, A facile one-step method for synthesizing a parallelogram-shaped single-crystalline ZnO nanosheet, *Mater. Sci. Eng., B*, 2014, **184**, 1–6.

25 M. M. Rahman, S. B. Khan, H. M. Marwani, A. M. Asiri, K. A. Alamry, M. A. Rub, A. Khan, A. A. P. Khan and N. Azuma, Facile synthesis of doped ZnO–CdO nanoblocks as solid-phase adsorbent and efficient solar photo-catalyst applications, *J. Ind. Eng. Chem.*, 2014, **20**, 2278–2286.

26 K. Gurumurugan, D. Mangalaraj and S. K. Narayandass, Photodiode Based on CdO Thin Films as Electron Transport Layer, *J. Electron. Mater.*, 1996, **25**, 76543–76547.

27 F. T. Thema, P. Beukes, A. G. Fakim and M. Maaza, Green synthesis of monteponite CdO nanoparticles by *Agathosma betulina* natural extract, *J. Alloys Compd.*, 2015, **646**, 1043–1048.

28 T. Gutul, E. Rusu, N. Condur, V. Ursaki, E. Goncearenco and P. Vlazan, Preparation of poly(*N*-vinylpyrrolidone)-stabilized ZnO colloid nanoparticles, *Beilstein J. Nanotechnol.*, 2014, **5**, 402–406.

29 V. Bilgin, I. Akyuz, S. Kose and F. Atay, Characterization of Mn-incorporated CdO films grown by ultrasonic spray pyrolysis, *Semicond. Sci. Technol.*, 2006, **21**, 579–585.

30 W. S. Song, G. X. Y. Huang, R. C. Dai, Z. P. Wang and Z. M. Zhang, Raman scattering and photoluminescence investigation of YBO_3:Eu^{3+} under high temperature and high pressure, *J. Mater. Chem. C*, 2015, **3**, 2405–2412.

31 R. L. McCreery, *Raman Spectroscopy for Chemical Analysis*, John Wiley & Sons, Inc., 2000, 1st edn, pp. 1–420.

32 V. S. Bagal, G. P. Patil, A. B. Deore, S. R. Suryawanshi, D. J. Late, M. A. More and P. G. Chavan, Surface modification of aligned CdO nanosheets and their enhanced field emission properties, *RSC Adv.*, 2016, **6**, 41261–41267.

33 J. Haeberle, K. Henkel, H. Gargouri, F. Naumann, B. Gruska, M. Arens, M. Tallarida and D. Schmeißer, Ellipsometry and

XPS comparative studies of thermal and plasma enhanced atomic layer deposited Al_2O_3-films, *Beilstein J. Nanotechnol.*, 2013, **4**, 732–742.

34 H. L. Lee, I. A. Mohammed, M. Belmahi, M. B. Assouar, H. Rinnert and M. Alnot, Thermal and Optical Properties of CdS Nanoparticles in Thermotropic Liquid Crystal Monomers, *Materials*, 2010, **3**, 2069–2086.

35 D. Xu, D. Fan and W. Shen, Catalyst-free direct vapor-phase growth of $Zn_{1-x}Cu_xO$ micro-cross structures and their optical properties, *Nanoscale Res. Lett.*, 2013, **8**, 46.

36 F. Zhang, X. Wu, C. Liang, X. Li, Z. Wang and H. Li, Highly active, water-compatible and easily separable magnetic mesoporous Lewis acid catalyst for the Mukaiyama-Aldol reaction in water, *Green Chem.*, 2014, **16**, 3768–3777.

37 Q. Yin, X. Jin, G. Yang, C. Jiang, Z. Song and G. Sun, Biocompatible folate-modified Gd^{3+}/Yb^{3+}doped ZnO nanoparticles for dual modal MRI/CT imaging, *RSC Adv.*, 2014, **4**, 53561–53569.

38 S. D. Kapse, F. C. Raghuwanshi, V. D. Kapse and D. R. Patil, Characteristics of high sensitivity ethanol gas sensors based on nanostructured spinel $Zn_{1-x}Co_xAl_2O_4$, *Curr. Appl. Phys.*, 2012, **12**, 307–312.

39 M. M. Abdullah, M. M. Rahman, H. Bouzid, M. Faisal, S. B. Khan, S. A. Al-Sayari and A. A. Ismail, Sensitive and fast response ethanol chemical sensor based on as-grown Gd_2O_3 nanostructures, *J. Rare Earths*, 2015, **33**, 214–220.

40 A. Mirzaei, K. Janghorban, B. Hashemi, M. Bonyani, S. G. Leonardi and G. Neri, Highly stable and selective ethanol sensor based on α-Fe_2O_3 nanoparticles prepared by Pechini sol–gel method, *Ceram. Int.*, 2016, **42**, 6136–6144.

41 S. Roy, N. Banerjee, C. K. Sarkar and P. Bhattacharyya, Development of an ethanol sensor based on CBD grown ZnO nanorods, *Solid-State Electron.*, 2013, **87**, 43–50.

42 M. Faisal, S. B. Khan, M. M. Rahman, A. Jamal and A. Umar, Ethanol chemi-sensor: Evaluation of structural, optical and sensing properties of CuO nanosheets, *Mater. Lett.*, 2011, **65**, 1400–1403.

43 M. Gholami, A. A. Khodadadi, A. A. Firooz and Y. Mortazavi, In_2O_3–ZnO nanocomposites: High sensor response and selectivity to ethanol, *Sens. Actuators, B*, 2015, **212**, 395–403.

44 W. Wang, Y. Tian, X. Li, X. Wang, H. He, Y. Xu and C. He, Enhanced ethanol sensing properties of Zn-doped SnO_2 porous hollow microspheres, *Appl. Surf. Sci.*, 2012, **261**, 890–895.

45 M. Faisal, S. B. Khan, M. M. Rahman, A. Jamal, A. M. Asiri and M. M. Abdullah, Smart chemical sensor and active photo-catalyst for environmental pollutants, *Chem. Eng. J.*, 2011, **173**, 178–184.

46 S. B. Khan, M. Faisal, M. M. Rahman and A. Jamal, Exploration of CeO_2 nanoparticles as a chemi-sensor and photo-catalyst for environmental applications, *Sci. Total Environ.*, 2011, **409**, 2987–2992.

47 M. Faisal, S. B. Khan, M. M. Rahman, A. Jamal and A. Umar, Ethanol chemi-sensor: Evaluation of structural, optical and sensing properties of CuO nanosheets, *Mater. Lett.*, 2011, **65**, 1400–1403.

48 M. M. Rahman and A. M. Asiri, Fabrication of highly sensitive ethanol sensor based on doped nanostructure materials using tiny chips, *RSC Adv.*, 2015, **5**, 63252–63262.

49 M. M. Rahman, A. Jamal, S. B. Khan and M. Faisal, Fabrication of highly sensitive ethanol chemical sensor based on Sm doped Co_3O_4 Nanokernels by a hydrothermal method, *J. Phys. Chem. C*, 2011, **115**, 9503–9510.

50 M. M. Abdullah, M. M. Rahman, M. Faisal, S. B. Khan, P. Singh, M. A. Rub, N. Azum, A. Khan, A. A. P. Khan and M. Hasmuddin, Fabrication of ethanol chemical sensors based on as-prepared Gd_2O_3 nanorods by facile hydrothermal routes, *J. Colloid Sci. Biotechnol.*, 2014, **2**, 322–327.

51 S. B. Khan, M. M. Rahman, K. Akhtar, A. M. Asiri, J. Seo, H. Han and K. Alamry, Novel and sensitive ethanol chemi-sensor based on nanohybrid materials, *Int. J. Electrochem. Sci.*, 2012, **7**, 4030–4038.

52 P. Song, H. W. Qin, L. Zhang, K. An, Z. J. Lin, J. F. Hu and M. H. Jiang, The structure, electrical and ethanol-sensing properties of $La_{1-x}Pb_xFeO_3$ perovskite ceramics with $x \leq 0.3$, *Sens. Actuators, B*, 2005, **104**, 312–316.

53 T. J. Hsueh, C. L. Hsu, S. J. Chang and I. C. Chen, Laterally grown ZnO nanowire ethanol gas sensors, *Sens. Actuators, B*, 2007, **126**, 473–477.

54 B. Tao, J. Zhang, S. Hui and L. Wan, *Sens. Actuators, B*, 2009, **142**, 298.

55 E. Wongrat, P. Pimpang and S. Choopun, Comparative study of ethanol sensor based on gold nanoparticles: ZnO nanostructure and gold: ZnO nanostructure, *Appl. Surf. Sci.*, 2009, **256**, 968–971.

56 M. Faisal, S. B. Khan, M. M. Rahman and A. Jamal, Ethanol chemi-sensor: Evaluation of structural, optical and sensing properties of CuO nanosheets, *Mater. Lett.*, 2011, **65**, 1400–1403.

57 S. Mujumdar, Synthesis and characterization of SnO2 films obtained by a wet chemical process, *Mater. Sci.-Pol.*, 2009, **27**, 123–128.

58 J. Hagen, *Heterogeneous Catalysis: Fundamentals*, Wiley-VCH, Weinheim, 1999, vol. 83.

59 K. Sahner, R. Moos, M. Matam and J. J. Tunney, Hydrocarbon sensing with thick and thin film p-type conducting perovskite materials, *Sens. Actuators, B*, 2005, **108**, 102–112.

60 S. Pokrel, C. E. Simon, V. Quemener, N. Bârsan and U. Weimer, Investigations of conduction mechanism in Cr_2O_3 gas sensing thick films by ac impedance spectroscopy and work function changes measurements, *Sens. Actuators, B*, 2008, **133**, 78–83.

61 C. Wang, X. Q. Fu, X. Y. Xue, Y. G. Wang and T. H. Wang, Surface accumulation conduction controlled sensing characteristic of p-type CuO nanorods induced by oxygen adsorption, *Nanotechnology*, 2007, **18**, 145506.

62 H. Nanto, H. Sokooshi and T. Usuda, *Solid-State Sens. Actuators*, 1991, **24–27**, 596.

63 O. Schmidt, P. Kiesel, C. G. Van de Walle, N. M. Johnson, J. Nause and G. H. Dohler, *Jpn. J. Appl. Phys., Part 1*, 2005, **44**, 7271.

64 O. Schmidt, A. Geis, P. Kiesel, C. G. Van de Walle, N. M. Johnson, A. Bakin, A. Waag and G. H. Dohler, *Superlattices Microstruct.*, 2006, **39**, 8.
65 D. C. Look, *Surf. Sci.*, 2007, **601**, 5315.
66 S. E. Harrison, *Phys. Rev.*, 1954, **93**, 52.
67 A. R. Hutson, *Phys. Rev.*, 1957, **108**, 222.
68 A. Janottic and C. G. Van de Walle, *Rep. Prog. Phys.*, 2009, **72**, 126501.